

Research



Cite this article: Tam A, Green JEF, Balasuriya S, Tek EL, Gardner JM, Sundstrom JF, Jiranek V, Binder BJ. 2019 A thin-film extensional flow model for biofilm expansion by sliding motility. *Proc. R. Soc. A* **475**: 20190175. <http://dx.doi.org/10.1098/rspa.2019.0175>

Received: 21 March 2019

Accepted: 22 July 2019

Subject Areas:

applied mathematics, mathematical modelling, fluid mechanics

Keywords:

Saccharomyces cerevisiae, yeast, mat formation experiments, lubrication theory, multi-phase flow, viscous flow

Author for correspondence:

Alexander Tam

e-mail: alexander.tam@adelaide.edu.au

Electronic supplementary material is available online at <https://doi.org/10.6084/m9.figshare.c.4614143>.

A thin-film extensional flow model for biofilm expansion by sliding motility

Alexander Tam¹, J. Edward F. Green¹,

Sanjeeva Balasuriya¹, Ee Lin Tek²,

Jennifer M. Gardner², Joanna F. Sundstrom²,

Vladimir Jiranek² and Benjamin J. Binder¹

¹School of Mathematical Sciences, University of Adelaide, Adelaide, South Australia 5005, Australia

²Department of Wine and Food Science, Waite Campus, University of Adelaide, Urrbrae, South Australia 5064, Australia

AT, 0000-0003-3565-1068

In the presence of glycoproteins, bacterial and yeast biofilms are hypothesized to expand by sliding motility. This involves a sheet of cells spreading as a unit, facilitated by cell proliferation and weak adhesion to the substratum. In this paper, we derive an extensional flow model for biofilm expansion by sliding motility to test this hypothesis. We model the biofilm as a two-phase (living cells and an extracellular matrix) viscous fluid mixture, and model nutrient depletion and uptake from the substratum. Applying the thin-film approximation simplifies the model, and reduces it to one-dimensional axisymmetric form. Comparison with *Saccharomyces cerevisiae* mat formation experiments reveals good agreement between experimental expansion speed and numerical solutions to the model with $\mathcal{O}(1)$ parameters estimated from experiments. This confirms that sliding motility is a possible mechanism for yeast biofilm expansion. Having established the biological relevance of the model, we then demonstrate how the model parameters affect expansion speed, enabling us to predict biofilm expansion for different experimental conditions. Finally, we show that our model can explain the ridge formation observed in some biofilms. This is especially true if surface tension is low, as hypothesized for sliding motility.

1. Introduction

Micro-organisms can form colonies with fascinating and complex spatio-temporal patterns. As these colonies are readily grown in experiments, bacteria and fungi are often used as model organisms to investigate the mechanisms of pattern formation in large collections of cells. Identifying the contributions of different candidate mechanisms to the self-organization process is an important problem in developmental biology [1]. For example, Turing [2] and Keller & Segel [3] famously showed that heterogeneous patterns can develop from a homogeneous initial state as a result of reaction and diffusion of chemicals. Murray [1] proposed a more general mechanochemical theory, where chemical signals combine with mechanical interactions between cells and their environment to give rise to spatial patterns. As these mechanisms can interact in a complex manner, pattern formation in micro-organisms continues to be an active field of research.

Reynolds & Fink [4] showed that the bakers' yeast *Saccharomyces cerevisiae* can form mats when grown on semi-solid agar. These mats consist of cells embedded in a self-produced extracellular matrix (ECM), and established *S. cerevisiae* as a useful model organism for fungal biofilm formation. We previously showed that a minimal reaction–diffusion model for nutrient-limited growth alone could reproduce the floral pattern observed in mat formation experiments [5]. However, experimental observations also led Reynolds & Fink [4] to hypothesize that yeast biofilms expand by sliding motility. This involves a sheet of cells spreading as a unit due to the expansive forces of cell growth [6], and reduced friction between the cells and substratum [7], and is not considered in previous models.

In this work, we use a combination of mathematical modelling and experiments to investigate the extent to which sliding motility contributes to yeast biofilm formation. In §1a,b, we review the existing literature on yeast biofilms and the mathematical modelling thereof. In §2, we derive a two-phase (living cells and the ECM) mathematical model for biofilm expansion. We then exploit the thin biofilm geometry to obtain a one-dimensional, radially symmetric thin-film approximation to the general model in §3. We compute numerical solutions to the thin-film model in §4, and show that it can reproduce the expansion speed observed in experiments. We confirm that cell proliferation drives expansion in sliding motility, and demonstrate how the movement, uptake and consumption of nutrients affect expansion speed. We close the paper in §5, concluding that sliding motility is a plausible mechanism for biofilm formation in yeast.

(a) Biological background

A biofilm is a slimy community of micro-organisms existing on a surface, in which cells adhere to each other and reside within a self-produced ECM. An estimated 80% of bacteria in nature exists in biofilm colonies [8]. For this reason, they have been described as the 'oldest, most successful and widespread form of life on Earth' [9], and have attracted significant research attention. Our main objective is to better understand the mechanisms of yeast biofilm expansion. Yeasts are single-cell fungal organisms that have well-known everyday uses, for example, in baking and brewing. However, yeast species such as the pathogenic *Candida albicans*, often form biofilms on indwelling medical devices [10]. These biofilms are a leading cause of infections in clinical settings, and can be up to 2000 times more resistant to anti-fungal agents than planktonic cells [8]. Inability to remove fungal biofilms can lead to candidiasis, which is an invasive disease estimated to affect around 0.2% of the population per year. Due to its high resistance to treatment, candidiasis has a mortality rate of 30–40% in immunocompromised people [11]. However, despite these significant impacts on human health, fungal biofilms are much less widely studied than bacterial biofilms [12].

The ECM is a distinguishing feature of biofilms. It consists of water, which forms up to 97% of matrix material [13], and various extracellular polymeric substances (EPS). Although the composition and function of the ECM may differ between species, it provides biofilm colonies with several advantages over planktonic cells, as summarized by Flemming & Wingender [9]. For yeast biofilms specifically, the ECM has been observed to assist the transportation of

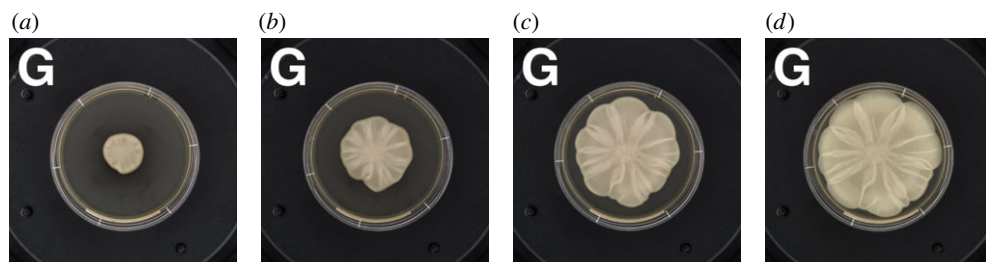


Figure 1. A time series of images from a *S. cerevisiae* mat formation experiment [5] ((a) 68 h, (b) 117 h, (c) 164 h and (d) 237 h). (Online version in colour.)

nutrients [14], and prevent penetration of harmful external substances [15]. The ECM also influences biofilm rheology. Although biofilms are viscoelastic in general, on time scales longer than the order of minutes they tend to behave as viscous fluids [9,16,17].

The budding yeast *Saccharomyces cerevisiae* has emerged as a useful model for fungal biofilm growth in cell biology research [4]. A major advantage of using *S. cerevisiae* in experiments is that its genome has been sequenced [18], and a wide variety of genetic tools such as mutant libraries are available. As it is closely related to *C. albicans* [19], it has assumed an important role in the identification of new targets for anti-fungal therapy [4,20]. Furthermore, as a eukaryotic organism its basic cellular processes also have a lot in common with human cells [20]. Due to this, *S. cerevisiae* has also been used as a model for understanding the division of cancer cells [12].

Reynolds & Fink [4] were the first to perform mat formation experiments with *S. cerevisiae*, and similar methods have been used in subsequent studies [5,12,21]. In these experiments, yeast cells are inoculated on semi-solid (0.3%) agar plates. They initially form a thin round biofilm, which over time expands and forms a complex mat structure, characterized by petal-like features at its edge. This transition is illustrated in figure 1.

A notable finding of Reynolds & Fink [4] is that the glycoprotein Flo11p is required for mat formation. Similar glycopeptidolipids are prerequisites for biofilm formation in *Mycobacterium smegmatis*. This is because they increase cell surface hydrophobicity, which results in weak adhesion between the biofilm and substratum [7]. Furthermore, *S. cerevisiae* cells are non-motile [22], making them unable to respond actively to nutrient or chemical gradients. Reynolds and Fink subsequently hypothesized that sliding motility, which is a form of passive growth, is the driving mechanism of yeast biofilm formation. Recent studies on bacterial biofilms have also revealed that osmotic swelling is another potential mechanism for biofilm expansion [23,24]. This requires production of EPS, which creates an osmotic pressure difference between the biofilm and environment. The biofilm then physically expands by taking up water from the agar [23]. The extent to which sliding motility and osmotic swelling contribute to expansion depends on the microbial species and environment [24]. For example, in some bacterial biofilms including *Bacillus subtilis*, in which ECM fraction is commonly 50–90% [25] and can be as high as 95–98% [13,26], osmotic swelling is the primary mechanism [23]. By contrast, we observe that ECM fraction is approximately 10% in *S. cerevisiae* mats, suggesting that cell proliferation and sliding motility will play a larger role. However, no detailed study into whether sliding motility is the mechanism of yeast biofilm expansion has been performed. Investigating this is the subject of our paper.

(b) Previous models of biofilm formation

Owing to their ubiquity and importance to infections, biofilms have attracted significant attention in the applied mathematics community. Previous models have incorporated a wide variety of approaches (see Mattei *et al.* [25] for a comprehensive recent review). These include agent-based or hybrid models [27–29], and reaction–diffusion systems [5,12,30–32], both of which model the spread of cells, and movement and consumption of nutrients. However, a limitation of both

of these approaches is that it is difficult to include the effect of colony mechanics, such as extracellular fluid flow. As modelling sliding motility requires considering the ECM mechanics, we restrict our attention here to models that incorporate the extracellular fluid.

In the literature, many authors include external fluid flow when modelling biofilm growth. A common approach is to consider biofilms immersed in a liquid culture medium, growing perpendicular to non-reactive, impermeable substrata. These models then incorporate the hydrodynamics of bulk fluid in the medium [33–35]. We focus primarily on another promising approach, in which biofilm constituents are themselves treated as fluids [36,37]. Under this framework, biofilms are typically modelled as multi-phase mixtures of cells, EPS and external liquid [17,26,38–43]. Applying conservation of mass and momentum for each fluid phase then enables the mechanics of each fluid, and interactions between phases, to be taken into account.

We aim to model *S. cerevisiae* mat formation experiments, which involve a biofilm spreading radially by sliding motility, with nutrients supplied from the agar substratum. The radius of these yeast biofilms significantly exceeds their height, which makes thin-film models well suited to this problem. In most previous models that adopt the thin-film approximation in multi-phase fluid models, the authors derive a fourth-order generalized lubrication equation for the evolution of the biofilm height [22,23,44–50]. These models can then incorporate additional features, to investigate the effects of nutrient supply [44,45,47,50,51], osmotic swelling [23,47,50], quorum sensing [46] and surface forces [47–49] on biofilm growth. However, a common feature of these models is that the derivation of a generalized lubrication equation requires the assumption of strong adhesion between the biofilm and substratum. As a result, flow is driven by a large pressure that must be balanced with a comparatively large surface tension. By contrast, sliding motility involves increased cell surface hydrophobicity, and hence weak adhesion between the biofilm and agar. Modelling *S. cerevisiae* mat formation therefore requires an alternative approach.

The model of Ward & King [46] is of particular interest to the problem of biofilm expansion by sliding motility. They treat a bacterial biofilm as a multi-phase mixture of cells and water, and use an extensional flow thin-film reduction to derive a model for the early time spread of the colony. This approach assumes weak adhesion between the biofilm and substratum and is therefore well-suited to modelling the sliding motility mechanism. However, in their model the biofilm is immersed in a nutrient-rich liquid culture medium. This is unlike *S. cerevisiae* mats, which receive nutrients from the agar substratum; their ability to spread therefore depends on the supply of a depleting nutrient, which is also relevant to biofilm growth in nature or in a human host [52]. Ward & King [46] also only consider early biofilm development, and thus neglect ECM production and spatio-temporal variation in the cell volume fraction, which become important on the time scale of our experiments. Furthermore, multi-phase fluid models have also only previously been applied to bacterial biofilms, rather than the fungal biofilms considered here. Based on these considerations, we aim to extend the thin-film model of Ward & King [46], to model *S. cerevisiae* mat formation experiments.

2. Mathematical model

We consider growth of a yeast biofilm in cylindrical co-ordinates (r, θ, z) , and assume radial symmetry from the outset. The biofilm occupies the region $0 < r < S(t)$ and $0 < z < h(r, t)$, where the leading edge of the biofilm $S(t)$ is termed the contact line, and $h(r, t)$ represents the biofilm–air interface, which is a free surface. We define H_b and R_b to be the characteristic height and radius of biofilm growth, respectively. The biofilm grows on a substratum, which has depth H_s and is assumed rigid. A sketch of the problem domain, which closely resembles that of Ward & King [46], is shown in figure 2.

We adopt a macroscopic continuum model, and treat the biofilm as a mixture of two viscous fluid phases. These are a living cell phase denoted with the subscript n , and an ECM phase denoted with the subscript m . We define the volume fractions of living cells and ECM to be

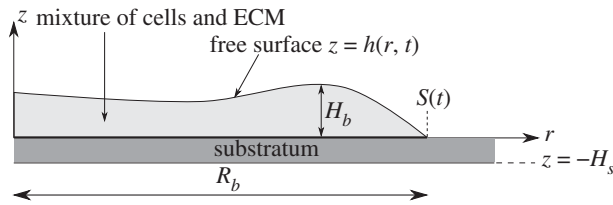


Figure 2. Diagram illustrating a vertical slice through the centre of the biofilm and substratum.

$\phi_n(r, z, t)$ and $\phi_m(r, z, t)$, respectively, and assume that the mixture contains no voids, that is

$$\phi_n + \phi_m = 1. \quad (2.1)$$

In defining these volume fractions, we note that it is not possible for both species to occupy the same space simultaneously. Throughout this work, we implicitly assume that an appropriate averaging process has taken place, and do not discuss the details here. We direct the reader to the paper by Drew [53] for further information.

A novelty of our approach is that we combine a thin-film extensional flow model for sliding motility with nutrient uptake from a depleting supply in the substratum. To enable this, we introduce $g_s(r, z, t)$, the nutrient concentration in the substratum defined for $-H_s < z < 0$, and $g_b(r, z, t)$, the nutrient concentration in the biofilm, defined for $0 < z < h(r, t)$ and $0 < r < S(t)$. After deriving the governing equations, we impose the initial and boundary conditions required to close the model in §2b. Nutrients can enter the biofilm across the biofilm–substratum interface, at which point they become available for consumption by the cells. This, combined with boundary conditions for the fluid flow, completes our description of sliding motility in biofilms.

(a) Governing equations

We derive the governing equations of our general model using conservation of mass and momentum. For the mass balances, we assume that the density of each fluid phase is constant, and that the mass flux of each phase is entirely advective. The mass balance equations then read

$$\frac{\partial \phi_\alpha}{\partial t} + \frac{1}{r} \frac{\partial}{\partial r} (r u_{r\alpha} \phi_\alpha) + \frac{\partial}{\partial z} (u_{z\alpha} \phi_\alpha) = J_\alpha, \quad (2.2)$$

where $\mathbf{u}_\alpha = (u_{r\alpha}, u_{z\alpha})$ for $\alpha = n, m$, are the fluid velocities. The J_α terms represent the net volumetric source of phase α . For these terms, we adapt the bilinear forms used in Tam *et al.* [5] to include cell death. Assuming that dead cells immediately become part of the ECM, we write

$$J_n = \psi_n \phi_n g_b - \psi_d \phi_n \quad \text{and} \quad J_m = \psi_m \phi_n g_b + \psi_d \phi_n, \quad (2.3)$$

where ψ_n is the cell production rate, ψ_m is the ECM production rate and ψ_d is the cell death rate, all of which are constant. In (2.3), cell death is proportional to cell density only, while production of both living cells and ECM increases with local cell density and nutrient concentration. This is consistent with experimental observations, which show that cellular components and ECM are both formed by catabolism of cellular synthesized glucose [54]. Despite not being considered here, our model also retains the possibility of incorporating more complicated mechanisms, for example, ECM production regulated by quorum sensing [39].

We assume that nutrients disperse by diffusion in the substratum, and by both diffusion and advection with extracellular fluid inside the biofilm. As in Tam *et al.* [5], we assume that the rate at which nutrients are consumed is proportional to the local density of cells and nutrients. The mass balance equations for the nutrients in the substratum and biofilm, respectively, then read

$$\frac{\partial g_s}{\partial t} = D_s \left[\frac{1}{r} \frac{\partial}{\partial r} \left(r \frac{\partial g_s}{\partial r} \right) + \frac{\partial^2 g_s}{\partial z^2} \right] \quad (2.4)$$

and

$$\frac{\partial g_b}{\partial t} + \frac{1}{r} \frac{\partial}{\partial r} [ru_{rm}(1 - \phi_n)g_b] + \frac{\partial}{\partial z} [u_{zm}(1 - \phi_n)g_b] = D_b \left[\frac{1}{r} \frac{\partial}{\partial r} \left(r \frac{\partial g_b}{\partial r} \right) + \frac{\partial^2 g_b}{\partial z^2} \right] - \eta \phi_n g_b, \quad (2.5)$$

where D_s and D_b are the nutrient diffusivities in the substratum and biofilm, respectively, and η is the maximum nutrient consumption rate.

Since the biofilm spreads as a unit in sliding motility, we follow O’Dea *et al.* [55] in assuming strong interphase drag between the cells and the ECM, so that both phases move with the same velocity $\mathbf{u}_n = \mathbf{u}_m = \mathbf{u}$. Then, for simplicity we assume that the cells and ECM have the same dynamic viscosity μ , so effectively the mixture can be treated as a single viscous fluid. We denote the stress tensor for the mixture by $\boldsymbol{\sigma}$, and since inertial effects are negligible ($\text{Re} \ll 1$) on the time and length scales of biofilm growth, it satisfies the momentum balance equation

$$\nabla \cdot \boldsymbol{\sigma} = \mathbf{0}. \quad (2.6)$$

Owing to cell proliferation and death, and ECM production, the stress components for the mixture will include terms involving $\nabla \cdot \mathbf{u}$, which commonly vanish. In cylindrical geometry, the relevant components of the stress tensor are

$$\left. \begin{aligned} \sigma_{rr} &= -p - \frac{2\mu}{3} \nabla \cdot \mathbf{u} + 2\mu \frac{\partial u_r}{\partial r}, & \sigma_{rz} &= \sigma_{zr} = \mu \left(\frac{\partial u_r}{\partial z} + \frac{\partial u_z}{\partial r} \right) \\ \sigma_{\theta\theta} &= -p - \frac{2\mu}{3} \nabla \cdot \mathbf{u} + \frac{2\mu}{r} u_r, & \sigma_{zz} &= -p - \frac{2\mu}{3} \nabla \cdot \mathbf{u} + 2 \frac{\partial u_z}{\partial z}. \end{aligned} \right\} \quad (2.7)$$

and

where p is the pressure [56]. Note that we have invoked Stokes’ hypothesis, giving the standard coefficient $-2\mu/3$ for the divergence terms in (2.7) [17,46,57,58]. Substituting (2.7) into (2.6), we find that the momentum balances in the r - and z -directions, respectively, are

$$-\frac{\partial p}{\partial r} + \frac{2\mu}{r} \frac{\partial}{\partial r} \left(r \frac{\partial u_r}{\partial r} \right) - \frac{2\mu}{3} \frac{\partial}{\partial r} \left[\frac{1}{r} \frac{\partial}{\partial r} (ru_r) + \frac{\partial u_z}{\partial z} \right] + \mu \frac{\partial}{\partial z} \left(\frac{\partial u_z}{\partial r} + \frac{\partial u_r}{\partial z} \right) - \frac{2\mu}{r^2} u_r = 0 \quad (2.8a)$$

and

$$-\frac{\partial p}{\partial z} + 2\mu \frac{\partial^2 u_z}{\partial z^2} - \frac{2\mu}{3} \frac{\partial}{\partial z} \left[\frac{1}{r} \frac{\partial}{\partial r} (ru_r) + \frac{\partial u_z}{\partial z} \right] + \frac{\mu}{r} \frac{\partial}{\partial r} \left[r \left(\frac{\partial u_r}{\partial z} + \frac{\partial u_z}{\partial r} \right) \right] = 0. \quad (2.8b)$$

Given appropriate initial and boundary conditions, these momentum balance equations (2.8), together with the mass balance equations (2.2), (2.4), (2.5), define a closed system of governing equations for the fluid pressure, fluid velocity and nutrient concentrations.

(b) Initial and boundary conditions

To close the system of governing equations, we require initial and boundary conditions for all of the physical variables. When constructing the general model, we will leave the initial conditions arbitrary. We obtain the first boundary condition by noting that nutrient cannot pass through the base of the substratum. As the substratum is assumed rigid, the no-flux condition is

$$\frac{\partial g_s}{\partial z} = 0, \quad \text{on } z = -H_s. \quad (2.9)$$

When the cells are plated, there is no nutrient in the biofilm. Therefore, the nutrient concentration is initially discontinuous across the biofilm–substratum interface. To enable cell proliferation and expansion, the biofilm takes up nutrients from the substratum. We assume that the flux of nutrients across the biofilm–substratum interface is proportional to the local concentration difference, and expect that in general consumption of nutrients in the biofilm will sustain this

difference. Assuming fluid cannot pass through the interface, we then have

$$D_s \frac{\partial g_s}{\partial z} = -Q(g_s - g_b) \quad \text{and} \quad D_b \frac{\partial g_b}{\partial z} = -Q(g_s - g_b), \quad u_z = 0 \quad \text{on} \quad z = 0. \quad (2.10)$$

In equations (2.10), the constant Q is the nutrient mass transfer coefficient, which indicates the permeability of the biofilm. To obtain a condition for the fluid velocity on the biofilm–substratum interface, we use the hypothesis that sliding motility increases surface hydrophobicity, causing weak adhesion between the biofilm and substratum [6]. To model this, we impose zero tangential stress on the biofilm–substratum interface instead of the more common no-slip condition. The boundary condition reads

$$\hat{\mathbf{t}} \cdot (\phi_\alpha \boldsymbol{\sigma} \cdot \hat{\mathbf{n}}) = \frac{\partial u_r}{\partial z} + \frac{\partial u_z}{\partial r} = 0 \quad \text{on} \quad z = 0, \quad (2.11)$$

where $\hat{\mathbf{t}}$ is any unit tangent vector, and $\hat{\mathbf{n}}$ is the unit outward normal vector.

For the boundary conditions on the free surface, we first observe that nutrient cannot pass through the biofilm–air interface. This yields the no-flux condition

$$(g_b \phi_m \mathbf{u}_m - D_b \nabla g_b) \cdot \hat{\mathbf{n}} = 0 \quad \text{on} \quad z = h. \quad (2.12)$$

On each fluid phase, we also impose the kinematic condition

$$\frac{\partial h}{\partial t} + u_r \frac{\partial h}{\partial r} = u_z \quad \text{on} \quad z = h, \quad (2.13)$$

which states that fluid particles on the free surface must remain there. Finally, we obtain stress boundary conditions by noting that a free surface is subject to zero tangential stress, and normal stress that is proportional to its local curvature. In general, these conditions read

$$\hat{\mathbf{t}} \cdot (\phi_\alpha \boldsymbol{\sigma} \cdot \hat{\mathbf{n}}) = 0 \quad \text{and} \quad \hat{\mathbf{n}} \cdot (\phi_\alpha \boldsymbol{\sigma} \cdot \hat{\mathbf{n}}) = -\gamma \kappa \quad \text{on} \quad z = h, \quad (2.14)$$

where γ is the surface tension coefficient, and $\kappa = \nabla \cdot \hat{\mathbf{n}}$, for the free surface normal vector $\hat{\mathbf{n}} = (-h_r, 1)/(1 + h_r^2)^{-1/2}$ (where subscripts here denote partial differentiation), is the mean free surface curvature. This completes the boundary conditions associated with the model.

3. Extensional flow thin-film approximation

In this section, we use a thin-film approximation to obtain a simplified approximation to the model derived in §2. A key observation is that the radius of a biofilm significantly exceeds both its height and the depth of the substratum. This allows us to assume that the aspect ratio $H_s/R_b = \varepsilon \ll 1$, as well as $H_b/R_b = \mathcal{O}(\varepsilon)$. In §3a, we non-dimensionalize the governing equations with this in mind. The choice of scaling regime depends on the physics most relevant to the problem. For sliding motility in which surface tension is reduced [6], it is appropriate to model the biofilm as an extensional flow, which was considered by Ward & King [46]. In §3b,c, we adopt this approach, and use a thin-film approximation to simplify the governing equations and boundary conditions considerably. We then propose parameter values and source terms in §3d, yielding a one-dimensional axisymmetric model that we can compare with experimental results.

(a) Scaling and non-dimensionalization

To non-dimensionalize the equations, we use the initial biofilm radius, R_b , as the length scale, and scale time by the cell production rate, ψ_n , and initial nutrient concentration, G . The scaled

variables are (where hats denote dimensionless quantities)

$$\left. \begin{aligned} (r, z) &= (R_b \hat{r}, \varepsilon R_b \hat{z}), \quad (u_r, u_z) = (\psi_n GR_b \hat{u}_r, \varepsilon \psi_n GR_b \hat{u}_z) \\ \text{and} \quad t &= \frac{\hat{t}}{\psi_n G}, \quad g_s = G \hat{g}_s, \quad g_b = G \hat{g}_b, \quad p = \psi_n G \mu \hat{p}. \end{aligned} \right\} \quad (3.1)$$

Under this scaling, the governing equations (2.2), (2.4), (2.5) and (2.8) become, after dropping hats and eliminating ϕ_m by summing (2.2) over both phases and applying (2.1)

$$\frac{1}{r} \frac{\partial}{\partial r} (ru_r) + \frac{\partial u_z}{\partial z} = (1 + \Psi_m) \phi_n g_b, \quad (3.2a)$$

$$\frac{\partial \phi_n}{\partial t} + \frac{1}{r} \frac{\partial}{\partial r} (ru_r \phi_n) + \frac{\partial}{\partial z} (u_z \phi_n) = \phi_n g_b - \Psi_d \phi_n, \quad (3.2b)$$

$$\frac{\partial g_s}{\partial t} = D \left[\frac{1}{r} \frac{\partial}{\partial r} \left(r \frac{\partial g_s}{\partial r} \right) + \frac{1}{\varepsilon^2} \frac{\partial^2 g_s}{\partial z^2} \right], \quad (3.2c)$$

$$\begin{aligned} \text{Pe} \left\{ \frac{\partial g_b}{\partial t} + \frac{1}{r} \frac{\partial}{\partial r} [ru_r (1 - \phi_n) g_b] + \frac{\partial}{\partial z} [u_z (1 - \phi_n) g_b] \right\} \\ = \frac{1}{r} \frac{\partial}{\partial r} \left(r \frac{\partial g_b}{\partial r} \right) + \frac{1}{\varepsilon^2} \frac{\partial^2 g_b}{\partial z^2} - \Upsilon \phi_n g_b, \end{aligned} \quad (3.2d)$$

$$- \frac{\partial p}{\partial r} + \frac{2}{r} \frac{\partial}{\partial r} \left(r \frac{\partial u_r}{\partial r} \right) - \frac{2}{3} \frac{\partial}{\partial r} \left[\frac{1}{r} \frac{\partial}{\partial r} (ru_r) + \frac{\partial u_z}{\partial z} \right] + \frac{\partial}{\partial z} \left(\frac{\partial u_z}{\partial r} + \frac{1}{\varepsilon^2} \frac{\partial u_r}{\partial z} \right) - \frac{2u_r}{r^2} = 0 \quad (3.2e)$$

$$\text{and} \quad - \frac{\partial p}{\partial z} + 2 \frac{\partial^2 u_z}{\partial z^2} - \frac{2}{3} \frac{\partial}{\partial z} \left[\frac{1}{r} \frac{\partial}{\partial r} (ru_r) + \frac{\partial u_z}{\partial z} \right] + \frac{1}{r} \frac{\partial}{\partial r} \left[r \left(\frac{\partial u_r}{\partial z} + \varepsilon^2 \frac{\partial u_z}{\partial r} \right) \right] = 0, \quad (3.2f)$$

where we have introduced the dimensionless constants

$$\Psi_m = \frac{\psi_m}{\psi_n}, \quad \Psi_d = \frac{\psi_d G}{\psi_n}, \quad D = \frac{D_s}{\psi_n GR_b^2}, \quad \text{Pe} = \frac{\psi_n GR_b^2}{D_b} \quad \text{and} \quad \Upsilon = \frac{\eta R_b^2}{D_b}. \quad (3.3)$$

In (3.3), Ψ_m and Ψ_d are the dimensionless ECM production and cell death rates, respectively. The parameter D is the coefficient of diffusion for nutrients in the substratum, scaled by the cell production rate and biofilm radius. The Péclet number, Pe , is the ratio of the rates of advective transport to diffusive transport within the biofilm. The parameter Υ is the dimensionless nutrient consumption rate. We scale Υ differently to the corresponding term in Ward & King [46]. In their model, the biofilm was immersed in a nutrient-rich liquid culture medium, and hence they balanced nutrient consumption with diffusion in the z -direction. By contrast, *S. cerevisiae* mats grow on a nutrient-limited thin substratum, making it appropriate to balance nutrient consumption with the temporal derivative and in-plane advection and diffusion.

Applying the same scaling (3.1), the dimensionless boundary conditions are

$$\frac{\partial g_s}{\partial z} = 0, \quad \text{on } z = -1, \quad (3.4a)$$

$$\frac{\partial g_s}{\partial z} = -\varepsilon^2 Q_s (g_s - g_b), \quad \frac{\partial g_b}{\partial z} = -\varepsilon^2 Q_b (g_s - g_b) \quad \text{on } z = 0, \quad (3.4b)$$

$$\frac{\partial u_r}{\partial z} + \varepsilon^2 \frac{\partial u_z}{\partial r} = 0, \quad \text{on } z = 0, \quad (3.4c)$$

$$u_z = 0 \quad \text{on } z = 0, \quad u_z = \frac{\partial h}{\partial t} + u_r \frac{\partial h}{\partial r} \quad \text{on } z = h, \quad (3.4d)$$

$$\text{Pe} \left[g_b (1 - \phi_n) \left(u_r \frac{\partial h}{\partial r} - u_z \right) \right] = \frac{\partial g_b}{\partial r} \frac{\partial h}{\partial r} - \frac{1}{\varepsilon^2} \frac{\partial g_b}{\partial z} \quad \text{on } z = h, \quad (3.4e)$$

$$-2 \frac{\partial h}{\partial r} \left(\frac{\partial u_r}{\partial r} - \frac{\partial u_z}{\partial z} \right) + \frac{1}{\varepsilon^2} \frac{\partial u_r}{\partial z} + \frac{\partial u_z}{\partial r} - \left(\frac{\partial h}{\partial r} \right)^2 \left(\varepsilon^2 \frac{\partial u_z}{\partial r} + \frac{\partial u_r}{\partial z} \right) = 0 \quad \text{on } z = h \quad (3.4f)$$

and

$$-p + 2 \left[\varepsilon^2 \left(\frac{\partial h}{\partial r} \right)^2 + 1 \right]^{-1} \left[\varepsilon^2 \left(\frac{\partial h}{\partial r} \right)^2 \frac{\partial u_r}{\partial r} - \frac{\partial h}{\partial r} \left(\frac{\partial u_r}{\partial z} + \varepsilon^2 \frac{\partial u_z}{\partial r} \right) + \frac{\partial u_z}{\partial z} \right] - \frac{2}{3} \left[\frac{1}{r} \frac{\partial}{\partial r} (ru_r) + \frac{\partial u_z}{\partial z} \right] = -\gamma^* \kappa^* \quad \text{on } z = h, \quad (3.4g)$$

where κ^* is the dimensionless mean free surface curvature. The dimensionless parameters

$$Q_s = \frac{QR_b}{\varepsilon D_s}, \quad Q_b = \frac{QR_b}{\varepsilon D_b} \quad \text{and} \quad \gamma^* = \frac{\varepsilon \gamma}{\psi_n GR_b \mu} \quad (3.5)$$

are all assumed to be $\mathcal{O}(1)$. The mass transfer parameters Q_s and Q_b are the nutrient depletion rate (from the substratum), and nutrient uptake rate (by the biofilm), respectively. The dimensionless surface tension coefficient (or inverse capillary number), γ^* , is the ratio of surface tension forces to viscous forces. Equations (3.2), and the boundary conditions (3.4), then complete the dimensionless extensional flow model, on which we apply the thin-film reduction.

(b) Thin-film equations

We now use a thin-film approximation to simplify the dimensionless extensional flow model derived in §3a. This involves expanding the dependent variables in powers of ε^2

$$h(r, t) \sim h_0(r, t) + \varepsilon^2 h_1(r, t) + \mathcal{O}(\varepsilon^4) \quad (3.6a)$$

and

$$\phi_n(r, z, t) \sim \phi_{n0}(r, z, t) + \varepsilon^2 \phi_{n1}(r, z, t) + \mathcal{O}(\varepsilon^4), \quad (3.6b)$$

and so on, where series for p , u_r , u_z , g_s and g_b take the same form as (3.6b). Substituting (3.6) into the dimensionless governing equations (3.2), at leading order we obtain

$$\frac{1}{r} \frac{\partial}{\partial r} (ru_{r0}) + \frac{\partial u_{z0}}{\partial z} = (1 + \Psi_m) \phi_{n0} g_{b0}, \quad (3.7a)$$

$$\frac{\partial \phi_{n0}}{\partial t} + \frac{1}{r} \frac{\partial}{\partial r} (r\phi_{n0}u_{r0}) + \frac{\partial}{\partial z} (\phi_{n0}u_{z0}) = \phi_{n0}g_{b0} - \Psi_d \phi_{n0}, \quad (3.7b)$$

$$\frac{\partial^2 g_{s0}}{\partial z^2} = \frac{\partial^2 g_{b0}}{\partial z^2} = 0, \quad (3.7c)$$

$$\frac{\partial^2 u_{r0}}{\partial z^2} = 0 \quad (3.7d)$$

and

$$-\frac{\partial p_0}{\partial z} + \frac{1}{3} \frac{\partial}{\partial z} \left[\frac{1}{r} \frac{\partial}{\partial r} (ru_{r0}) + \frac{\partial u_{z0}}{\partial z} \right] + \frac{\partial^2 u_{z0}}{\partial z^2} = 0. \quad (3.7e)$$

These are subject to the leading-order boundary conditions

$$\frac{\partial g_{s0}}{\partial z} = 0 \quad \text{on } z = -1, 0, \quad \text{and} \quad \frac{\partial g_{b0}}{\partial z} = 0 \quad \text{on } z = 0, h_0, \quad (3.8a)$$

$$\frac{\partial u_{r0}}{\partial z} = 0 \quad \text{on } z = 0, h_0, \quad \text{and} \quad u_{z0} = 0 \quad \text{on } z = 0, \quad (3.8b)$$

$$\frac{\partial h_0}{\partial t} + u_{r0} \frac{\partial h_0}{\partial r} = u_{z0} \quad \text{on } z = h_0 \quad (3.8c)$$

and

$$-p_0 - \frac{2}{3r} \frac{\partial}{\partial r} (ru_{r0}) + \frac{4}{3} \frac{\partial u_{z0}}{\partial z} = \frac{\gamma^*}{r} \frac{\partial}{\partial r} \left(r \frac{\partial h_0}{\partial r} \right) \quad \text{on } z = h_0, \quad (3.8d)$$

where the rightmost term in (3.8d) incorporates $\kappa^* = \nabla^2 h_0$, which is the leading-order local free surface curvature.

Equations (3.7c), (3.7d) and the associated boundary conditions (3.8a), (3.8b) demonstrate that g_{s0} , g_{b0} and u_{r0} are independent of z , as is characteristic of extensional flows [59]. In a similar way to, for example King & Oliver [60], we exploit this by integrating the governing equations with respect to z across the biofilm depth to derive a one-dimensional closed system of equations for the leading-order variables. First, we introduce the depth-averaged cell volume fraction

$$\bar{\phi}_{n0} = \frac{1}{h_0} \int_0^{h_0} \phi_{n0} dz. \quad (3.9)$$

Integration of (3.7a), (3.7b) with respect to z then yields, after application of Leibniz's integral rule in (3.7b)

$$\frac{\partial h_0}{\partial t} + \frac{1}{r} \frac{\partial}{\partial r} (ru_{r0}h_0) = (1 + \Psi_m) \bar{\phi}_{n0} g_{b0} h_0 \quad (3.10a)$$

and

$$\frac{\partial}{\partial t} (\bar{\phi}_{n0} h_0) + \frac{1}{r} \frac{\partial}{\partial r} (ru_{r0} \bar{\phi}_{n0} h_0) = (\bar{\phi}_{n0} g_{b0} - \Psi_d \bar{\phi}_{n0}) h_0, \quad (3.10b)$$

where subtracting (3.10a) from (3.10b) gives

$$\frac{\partial \bar{\phi}_{n0}}{\partial t} + u_{r0} \frac{\partial \bar{\phi}_{n0}}{\partial r} = \bar{\phi}_{n0} [g_{b0} - \Psi_d - (1 + \Psi_m) \bar{\phi}_{n0} g_{b0}]. \quad (3.11)$$

To obtain equations for the leading-order nutrient concentrations, we need to consider the higher-order correction terms to the governing equations (3.2c) and (3.2d). Upon substituting the expansions (3.6), the $\mathcal{O}(1)$ balances are

$$\frac{\partial^2 g_{s1}}{\partial z^2} = \frac{1}{D} \frac{\partial g_{s0}}{\partial t} - \frac{1}{r} \frac{\partial}{\partial r} \left(r \frac{\partial g_{s0}}{\partial r} \right) \quad (3.12a)$$

and

$$\frac{\partial^2 g_{b1}}{\partial z^2} = \text{Pe} \left\{ \frac{\partial g_{b0}}{\partial t} + \frac{1}{r} \frac{\partial}{\partial r} [ru_{r0}(1 - \phi_{n0})g_{b0}] + \frac{\partial}{\partial z} [u_{z0}(1 - \phi_{n0})g_{b0}] \right\} - \frac{1}{r} \frac{\partial}{\partial r} \left(r \frac{\partial g_{b0}}{\partial r} \right) + \Upsilon \phi_{n0} g_{b0}. \quad (3.12b)$$

Using (3.4a), (3.4b) and (3.4e), we can also obtain higher-order corrections to the boundary conditions, giving

$$\frac{\partial g_{s1}}{\partial z} = 0 \quad \text{on } z = -1, \quad (3.13a)$$

$$\frac{\partial g_{s1}}{\partial z} = -Q_s (g_{s0} - g_{b0}), \quad \frac{\partial g_{b1}}{\partial z} = -Q_b (g_{s0} - g_{b0}) \quad \text{on } z = 0 \quad (3.13b)$$

and
$$\frac{\partial g_{b1}}{\partial z} = \frac{\partial g_{b0}}{\partial r} \frac{\partial h_0}{\partial r} - \text{Pe} g_{b0} (1 - \phi_{n0}) \left(u_{r0} \frac{\partial h_0}{\partial r} - u_{z0} \right) \quad \text{on } z = h_0. \quad (3.13c)$$

Integrating (3.12a) and (3.12b) with respect to z across the substratum and biofilm depth, respectively, and applying the boundary conditions (3.13), we obtain

$$\frac{\partial g_{s0}}{\partial t} = D \left[\frac{1}{r} \frac{\partial}{\partial r} \left(r \frac{\partial g_{s0}}{\partial r} \right) - Q_s (g_{s0} - g_{b0}) \right] \quad (3.14a)$$

and

$$\text{Pe} \left\{ h_0 \frac{\partial g_{b0}}{\partial t} + \frac{1}{r} \frac{\partial}{\partial r} [ru_{r0} (1 - \bar{\phi}_{n0}) g_{b0} h_0] \right\} = \frac{1}{r} \frac{\partial}{\partial r} \left(rh_0 \frac{\partial g_{b0}}{\partial r} \right) + Q_b (g_{s0} - g_{b0}) - \Upsilon \bar{\phi}_{n0} g_{b0} h_0, \quad (3.14b)$$

for $0 < r < S(t)$. We also need to take into account that the nutrient concentration in the substratum can be non-zero outside of the biofilm domain. Outside of the biofilm, the nutrient will disperse

via diffusion only, and therefore the mass balance equation outside of the biofilm is

$$\frac{\partial g_{s0}}{\partial t} = \frac{D}{r} \frac{\partial}{\partial r} \left(r \frac{\partial g_{s0}}{\partial r} \right), \quad \text{on } S(t) < r < R, \quad (3.15)$$

where $R = R_p/R_b$, and R_p is the radius of the Petri dish. We then seek a solution for g_{s0} such that the nutrient concentration and its first spatial derivative are both continuous at the contact line. Equations (3.14) and (3.15) then constitute the leading-order nutrient balance equations for our thin-film model.

Finally, we consider the higher-order correction term in the radial momentum equation (3.2e) to obtain equations for the leading-order radial velocity. Using the conservation of mass equation (3.2a) to simplify, the relevant term is

$$\frac{\partial^2 u_{r1}}{\partial z^2} = \frac{\partial p_0}{\partial r} + \frac{2}{3} (1 + \Psi_m) \frac{\partial}{\partial r} (\phi_{n0} g_{b0}) - \frac{2}{r} \frac{\partial}{\partial r} \left(r \frac{\partial u_{r0}}{\partial r} \right) - \frac{\partial}{\partial r} \left(\frac{\partial u_{z0}}{\partial z} \right) + \frac{2u_{r0}}{r^2}. \quad (3.16)$$

Similarly, the higher-order corrections to the boundary conditions (3.4c), (3.4f) are

$$\frac{\partial u_{r1}}{\partial z} = 0, \quad \text{on } z = 0 \quad \text{and} \quad \frac{\partial u_{r1}}{\partial z} = 2 \frac{\partial h_0}{\partial r} \left(\frac{\partial u_{r0}}{\partial r} - \frac{\partial u_{z0}}{\partial z} \right) - \frac{\partial u_{z0}}{\partial r} \quad \text{on } z = h_0. \quad (3.17)$$

To evaluate (3.16), we need to solve for the pressure p_0 . As u_{r0} is independent of z , integration of (3.7e) with respect to z yields, after applying (3.8d) and using (3.7a)

$$p_0 = \frac{4}{3} (1 + \Psi_m) \phi_{n0} g_{b0} - \frac{2}{r} \frac{\partial}{\partial r} (r u_{r0}) - \frac{\gamma^*}{r} \frac{\partial}{\partial r} \left(r \frac{\partial h_0}{\partial r} \right). \quad (3.18)$$

Now, integrating (3.16) with respect to z across the biofilm depth, and applying the boundary conditions (3.17), we obtain

$$4 \frac{\partial}{\partial r} \left[\frac{h_0}{r} \frac{\partial}{\partial r} (r u_{r0}) \right] - \frac{2u_{r0}}{r} \frac{\partial h_0}{\partial r} = 2 (1 + \Psi_m) \frac{\partial}{\partial r} (\bar{\phi}_{n0} g_{b0} h_0) - \gamma^* h_0 \frac{\partial}{\partial r} \left[\frac{1}{r} \frac{\partial}{\partial r} \left(r \frac{\partial h_0}{\partial r} \right) \right]. \quad (3.19)$$

Equations (3.10a), (3.11), (3.14), (3.15) and (3.19) then form a closed system for the leading-order biofilm height, (depth-averaged) cell volume fraction, nutrient concentrations and radial fluid velocity. These equations form our one-dimensional, thin-film extensional flow model.

(c) Initial and boundary conditions

We use experimental observations to propose initial and boundary conditions for the one-dimensional axisymmetric model. The experiments and procedure used in this work are described by Tam *et al.* [5]. In the experiments, the Petri dish is initially filled uniformly with nutrient, and a small droplet containing cells and fluid is inoculated in the centre of the dish using a pipette. The fluid in the droplet is rapidly absorbed into the agar substratum, leaving a thin layer of cells, which we assume adopts a parabolic profile. Experiments of *C. albicans* show that extracellular material only emerges in mature biofilm [61], hence we assume the biofilm is initially made up of cells only. Appropriate initial conditions are therefore

$$S(0) = 1, \quad h_0(r, 0) = H_0 (1 - r^2), \quad \bar{\phi}_{n0}(r, 0) = 1, \quad g_{s0}(r, 0) = 1 \quad \text{and} \quad g_{b0}(r, 0) = 0, \quad (3.20)$$

where H_0 is the initial biofilm height, which we expect to be $\mathcal{O}(\varepsilon)$. In specifying (3.20), we note that we have chosen the characteristic length scales to be the initial biofilm height and radius, and scale both nutrient concentrations by the initial concentration in the substratum.

For the boundary conditions, we first assume that the biofilm and nutrient concentration are radially symmetric, and that the centre of the biofilm is fixed. This yields the conditions

$$\frac{\partial h_0}{\partial r} \Big|_{(0,t)} = 0, \quad \frac{\partial \bar{\phi}_{n0}}{\partial r} \Big|_{(0,t)} = 0, \quad \frac{\partial g_{s0}}{\partial r} \Big|_{(0,t)} = 0 \quad \text{and} \quad \frac{\partial g_{b0}}{\partial r} \Big|_{(0,t)} = 0, \quad u_{r0}(0, t) = 0. \quad (3.21)$$

In addition, we know that the contact line position $S(t)$ evolves according to the local fluid velocity, that is

$$\frac{dS}{dt} = u_{r0}(S(t), t). \quad (3.22)$$

To close the one-dimensional axisymmetric model, we now require an additional boundary condition for each of the nutrient concentrations, and the fluid velocity. For the nutrient concentration in the substratum, it is natural to impose the no-flux condition

$$\left. \frac{\partial g_{s0}}{\partial r} \right|_{(R,t)} = 0 \quad (3.23)$$

at the boundary of the Petri dish. Regarding the nutrient concentration in the biofilm, we note that the leading edge of the biofilm is rounded by a meniscus, where the height changes over a region in r with $\mathcal{O}(\varepsilon)$ size [62]. This meniscus is not captured under the original thin-film scaling. With this in mind, close to the contact line we consider a re-scaling of the original variables

$$(r, z) = (S(t) + \varepsilon R_b r^\dagger, \varepsilon R_b z^\dagger) \quad \text{and} \quad (u_{r0}, u_{z0}) = (\varepsilon \psi_n G R_b u_{r0}^\dagger, \varepsilon \psi_n G R_b u_{z0}^\dagger). \quad (3.24)$$

With this scaling, the leading-order balance for the flux boundary condition (2.12) becomes (dropping daggers)

$$\frac{\partial g_{b0}}{\partial z} = \frac{\partial g_{b0}}{\partial r} \frac{\partial h_0}{\partial r} \quad \text{on } z = h_0. \quad (3.25)$$

At the contact line, the left-hand side of (3.25) vanishes due to (3.8a), and in general h_0 can depend on r . The boundary condition on the biofilm nutrient concentration is therefore

$$\left. \frac{\partial g_{b0}}{\partial r} \right|_{(S(t),t)} = 0. \quad (3.26)$$

To close the momentum equation (3.19), we impose that the biofilm experiences zero radial stress at the contact line, that is $\sigma_{rr}(S(t), t) = 0$. Using (3.18) to eliminate the pressure, we find that

$$\sigma_{rr} = 4 \frac{\partial u_{r0}}{\partial r} + 2 \frac{u_{r0}}{r} - 2(1 + \Psi_m) \phi_{n0} g_{b0} + \frac{\gamma^*}{r} \frac{\partial}{\partial r} \left(r \frac{\partial h_0}{\partial r} \right). \quad (3.27)$$

Integrating (3.27) over the biofilm depth, or noting that $\bar{\phi}_{n0} \rightarrow \phi_{n0}$ as $h \rightarrow 0$, we then obtain

$$4 \frac{\partial u_{r0}}{\partial r} + \frac{2u_{r0}}{r} = 2(1 + \Psi_m) \bar{\phi}_{n0} g_{b0} - \frac{\gamma^*}{r} \frac{\partial}{\partial r} \left(r \frac{\partial h_0}{\partial r} \right), \quad \text{on } (r, t) = (S(t), t). \quad (3.28)$$

Equations (3.10a), (3.11), (3.14), (3.15) and (3.19), together with the initial conditions (3.20) and boundary conditions (3.21), (3.22), (3.26), (3.28) and (3.23), form a closed one-dimensional axisymmetric model for leading-order variables. From here onwards, we drop zero subscripts on leading-order terms for convenience.

(d) Parameters

To obtain a set of parameters to use when comparing the model with *S. cerevisiae* mat formation experiments, we require estimates for all dimensional quantities in (3.1), (3.3) and (3.5). To assist with this, we first set $\Psi_m = 1/9$ to ensure that $\bar{\phi}_n$ will approach 0.9, as is consistent with experimental observation. For comparison purposes, we also set $\Psi_d = 0$, as cell death rate is difficult to measure, and images from the end of the experiments show that the proportion of dead cells is low. Furthermore, as reduced surface tension is a characteristic of sliding motility [6], we initially consider $\gamma^* = 0$. The experimental design then enables us to estimate all other dimensional parameters, with the exception of ψ_n and η , which we subsequently fit to experimental data. We then obtain the dimensionless parameters listed in table 1. Further details on how each was estimated are available in the electronic supplementary material. The parameter T corresponds to the dimensionless time taken to complete the experiment, and informs the time domain in numerical solutions to the model. We note that all constants in the right-hand column are $\mathcal{O}(1)$, which justifies the scaling regime employed in the thin-film model.

Table 1. Dimensionless parameter estimates for a yeast (*S. cerevisiae*) biofilm.

parameter	value	source	parameter	value	source
H_0	0.1	assumption	D	4.34	[63,64]
Ψ_m	0.111	observation	Pe	0.953	[65]
Ψ_d	0	observation	Υ	3.15	experimental data
R	14.4	experimental design	Q_b	8.65	[66]
T	15.9	experimental data	Q_s	2.09	[66]
γ^*	0	assumption			

4. Results and discussion

In this section, we compare the thin-film extensional flow model derived in §3 with experimental data, and then investigate the dependence of the parameters on the speed of biofilm expansion. To achieve this, we undertake the numerical solution of (3.10a), (3.11), (3.14), (3.15) and (3.19) on $r \in [0, R]$, and $t \in [0, T]$, subject to (3.21), (3.22), (3.26), (3.28), (3.23) and (3.20) in §4a. Doing so with the parameters in table 1 confirms that sliding motility can reproduce experimental results. In §4b,c, we then vary the parameters, including cell death rate and surface tension coefficient, to predict the expansion speed and biofilm shape in different conditions.

(a) Numerical solutions and comparison with experiments

We use a front-fixing method [67] to solve the one-dimensional axisymmetric model. This involves introducing the new variables

$$\xi = \frac{r}{S(t)} \quad \text{and} \quad \xi_o = \frac{r - S(t)}{R - S(t)}, \quad (4.1)$$

so that the biofilm always inhabits $\xi \in [0, 1]$, and the interval $\xi_o \in [0, 1]$ represents the remainder of the Petri dish not occupied by the biofilm. We then use a Crank–Nicolson scheme to discretize the model. For all nonlinear terms, we linearize using data from the previous time step. At each time step, we solve the governing equations in the same order as they are derived in §3b. When solving for the nutrient concentration in the substratum, we use data from the previous time step as an initial guess for $g_s(S, t)$ at the current time step. We then solve both (3.14a) and (3.15), and use Newton's method to correct the initial guess, and ensure that the first spatial derivative of g_s is continuous at $r = S(t)$, which corresponds to $\xi = 1$ and $\xi_o = 0$. We compute solutions using an equispaced grid with $\Delta\xi = \Delta\xi_o = 1.25 \times 10^{-4}$ and $\Delta t \approx 1 \times 10^{-4}$, which ensures adequate convergence with grid spacing and time step size. Further details on the numerical method are provided in the electronic supplementary material.

We compute solutions for the parameters given in table 1 to facilitate comparison with experiments. There is good agreement between the numerical contact line position and the measured radius of the *S. cerevisiae* mats, as shown in figure 3a. Unlike the reaction–diffusion model of Tam *et al.* [5], figure 3b shows that the extensional flow model produces a non-constant expansion speed. The velocity profile resembles the experimental *B. subtilis* biofilms of Srinivasan *et al.* [50], featuring an initial period of acceleration followed by a deceleration. A likely explanation of the acceleration observed early in biofilm growth is that cells initially proliferate in nutrient-rich conditions. With abundant nutrients, both existing and newly produced cells are able to proliferate, accelerating expansion. However, as time passes nutrients become depleted in the centre of the colony, as shown in figures 3c,d. When this occurs, cell proliferation is mostly confined to the leading edge (figure 3f), which slows the expansion of the colony. This phenomenon also dictates the shape a biofilm attains as it expands. As figure 3e shows, our model predicts that the biofilm will expand vertically and radially when nutrients are abundant. When

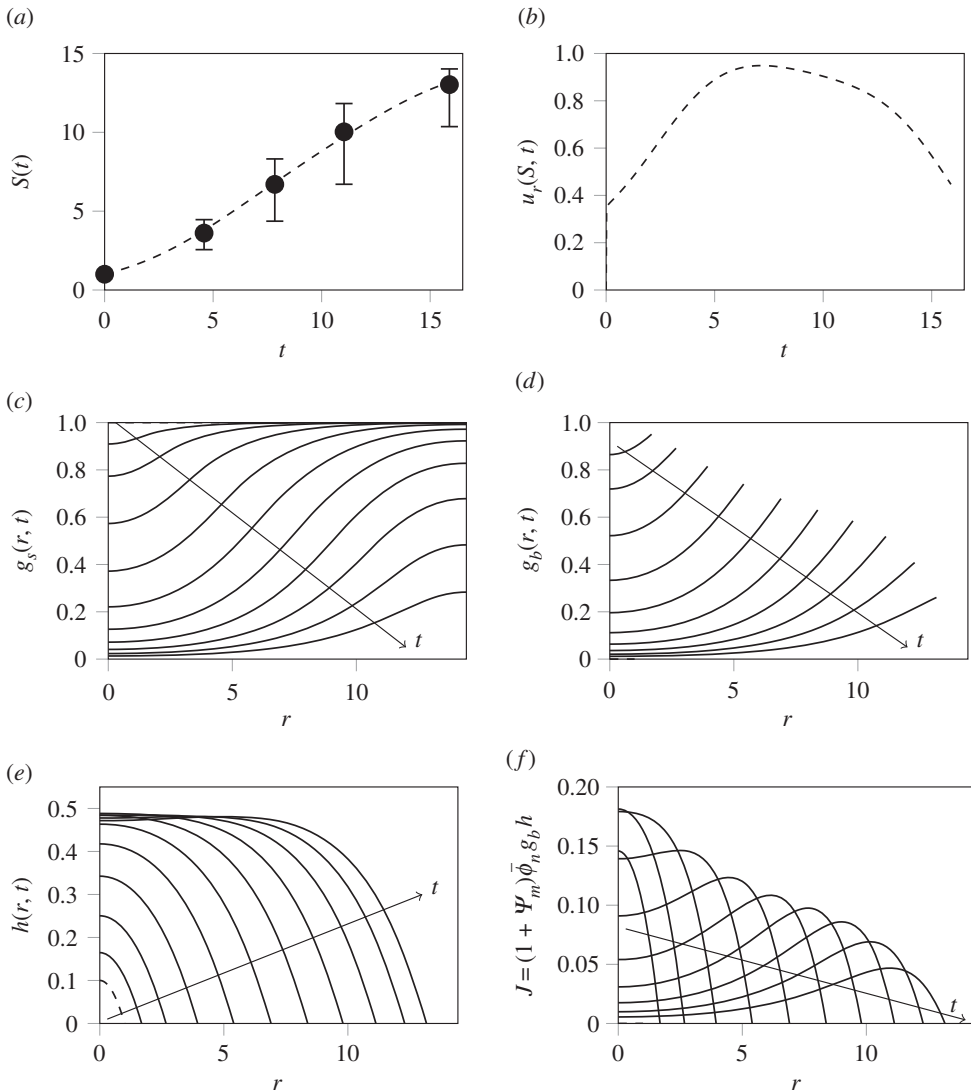


Figure 3. Numerical solution to the thin-film model, using parameters given in table 1, and comparison with experimental data. (a) Comparison of numerical contact line position (dashed curve) with experimental data. Dots indicate the mean data, and error bars indicate the experimental range. (b) Instantaneous biofilm expansion speed $u_r(S(t), t)$. (c–f) Spatio-temporal evolution of the model variables. Figures plotted for $t \in [0, 15.9]$, and $r \in [0, 14.4]$, at 10 equispaced time intervals. The dashed curve in (e) represents the initial condition, and arrows indicate the direction of increasing time. (c) Nutrient concentration (substratum), (d) nutrient concentration (biofilm), (e) biofilm height and (f) net fluid production.

nutrients deplete and growth is concentrated near the leading edge, the biofilm stops thickening and can only expand radially. The model even predicts that the height at the centre of the biofilm will begin to decrease slightly, as the advection of mass with the fluid exceeds the net production rate.

(b) The effect of model parameters on biofilm size

In §4a, we considered one set of parameters relevant to the *S. cerevisiae* mat formation experiments. However, biofilms can grow in vastly different ways depending on the microbial

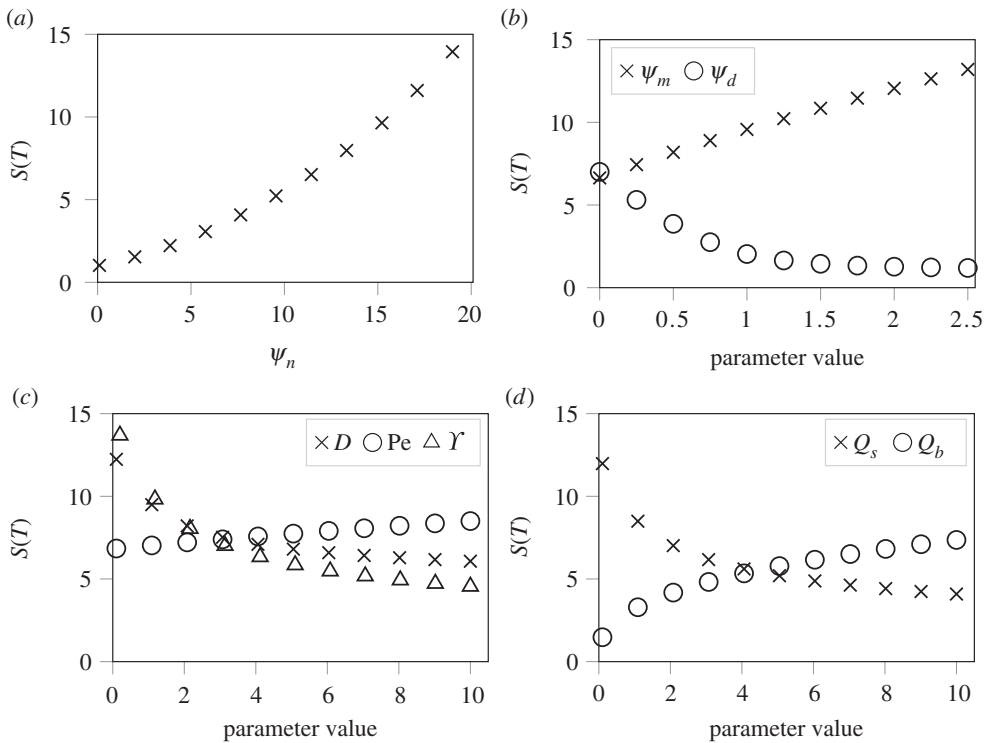


Figure 4. The effect of parameters on the predicted biofilm radius after 5 days of growth, $S(T)$. In each solution, we use the initial conditions (3.20). When held constant, all parameters (excepting T) are as in table 1. (a) The effect of cell production rate, ψ_n . (b) The effect of ECM production rate, Ψ_m , and cell death rate Ψ_d . (c) The effect of nutrient transport parameters, D , Pe and γ . (d) The effect of nutrient depletion and uptake parameters, Q_s , and Q_b .

species and environmental conditions. To predict biofilm growth by sliding motility in a range of experimental conditions, we compute numerical solutions for 5 days of growth. For each set of solutions, we use the default parameters given in table 1, and vary one parameter at a time over a realistic range. This allows us to isolate the effect of each parameter on biofilm size, and consequently expansion speed. Of the dimensionless parameters, we found that the Petri dish size R and surface tension coefficient γ^* had negligible effect on the biofilm size. Results for other dimensionless parameters and the cell production rate, ψ_n , are shown in figure 4. A vast range of behaviour is possible while keeping dimensionless parameters within one order of unity.

Figure 4a,b describes how fluid production and cell death affect expansion speed. As expected, higher rates of fluid (either living cells or ECM) production result in larger biofilms. However, unlike the production of ECM, the production of new cells facilitates increased cell proliferation in the future, and therefore cell production rate is a stronger determinant of size than ECM production rate. This verifies that expansion in sliding motility is mostly driven by cell proliferation. In addition, figure 4b shows that increasing the cell death rate decreases biofilm size, which is expected as fewer living cells are subsequently available to proliferate.

The remaining plots in figure 4 show how the dimensionless parameters affect expansion speed. The effect of nutrient movement and consumption is revealed in figure 4c. Increasing the nutrient diffusion coefficient D will result in more uniform nutrient concentrations across the Petri dish than seen in figure 3c,d. This promotes thickening of the biofilm as opposed to radial expansion. In addition, increasing the nutrient consumption rate γ results in larger quantities of nutrient being required to produce a new cell, thereby slowing expansion. The Péclet number indicates how readily nutrients advect radially with the extracellular fluid. Larger

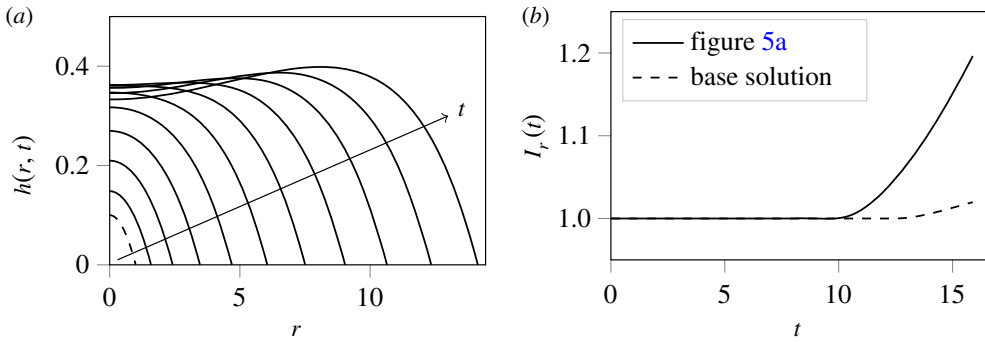


Figure 5. Numerical solution with $D = 1.5$, $\Upsilon = 10$ and $Pe = 10$, and other parameters as in table 1. (a) Spatio-temporal evolution of the biofilm height, illustrating the formation of a ridge near the leading edge. Figures plotted at 10 equispaced time intervals for $t \in [0, 15.9]$, where the dashed curve denotes the initial condition. (b) The normalized ridge height, I_r , confirming more pronounced ridge formation than the base solution in figure 3.

values of Pe increase nutrient supply to the proliferating rim, enabling faster expansion. However, the slender biofilm and substratum geometries are such that nutrient availability close to the leading edge depends more strongly on uptake from the substratum than advection in the biofilm. Therefore, the Péclet number has a weaker effect on expansion speed than the nutrient depletion and uptake rates, as figure 4d illustrates. Larger values of nutrient depletion rate Q_s decrease nutrient access to the cells, which slows expansion. Conversely, increasing nutrient uptake rate Q_b aids cell production, as more nutrients become available for consumption. A common theme in all of these results is that expansion speed depends on the ability of cells close to the leading edge to consume nutrient and proliferate. The results presented here are relevant to clinical settings, where expansion speed correlates with the invasiveness of infection. Our model describes environmental conditions that result in decreased expansion speed.

(c) Predicting biofilm shape: ridge formation and surface tension

In addition to the size, our model also predicts the shape a growing biofilm will attain. Although not observed in *S. cerevisiae* mat formation experiments, some bacterial biofilms [50] and yeast colony biofilms [54] develop a ridge structure close to the leading edge. To observe ridge formation in our model, we compute a numerical solution with the experimental parameters given in table 1, except with $D = 1.5$, $\Upsilon = 10$ and $Pe = 10$. Compared to the experimental parameters, this combination of decreased nutrient diffusion, and increased nutrient consumption and advection leads to faster nutrient depletion behind the proliferating rim. Cell proliferation then becomes concentrated close to the leading edge, which in conjunction with increased advection of mass outwards from the biofilm centre, creates the noticeable ridge seen in figure 5a. To quantify ridge formation, we compute the normalized ridge height $I_r(t) = (\max h(r, t))/h(0, t)$ in the new numerical solution, and compare with the experimental case. Figure 5b shows the normalized ridge height increasing faster than the base solution with experimental parameters. Although we do not investigate the mechanisms of ridge formation in detail, our model shows that interplay between sliding motility and nutrient-limited growth can initiate ridge formation. Importantly, this can occur without the need to invoke other mechanisms such as osmotic swelling or mechanical blistering.

Finally, we investigate the effect that non-zero surface tension would have on the biofilm shape. This surface tension represents the strength of cell–cell adhesion at the free surface, which we assumed weak when comparing with experiments. To investigate its effect, we compute numerical solutions with the parameters as in figure 5, while varying the surface tension coefficient over the range $\gamma^* \in [0, 2]$. These results are shown in figure 6. We observe

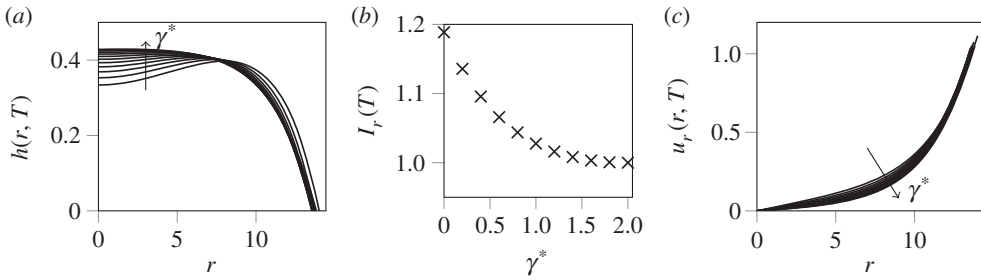


Figure 6. Numerical solutions with parameters (excepting γ^*) as in figure 5, illustrating how surface tension affects ridge formation. (a) Final biofilm height, $h(r, T)$, where $T = 15.9$, plotted for $\gamma^* \in [0, 2]$, at increments of $\gamma^* = 0.2$. (b) Normalized ridge height of the solutions in figure 6a, showing a decrease in ridge height with surface tension. (c) Instantaneous fluid velocity at $t = T$, again plotted for $\gamma^* \in [0, 2]$, at increments of $\gamma^* = 0.2$.

that increasing the surface tension coefficient reduces the extent of the ridge, and that $\gamma^* = 2$ is sufficient to prevent ridge formation. As surface tension appears only in the momentum equation (3.19) and boundary condition (3.28), we expect the fluid velocity profile to explain this behaviour. Figure 6c shows that increasing γ^* decreases the radial velocity near the centre of the biofilm. This decreases movement of fluid and nutrients towards the leading edge of the biofilm, thereby inhibiting ridge formation. However, we do not observe ridge formation in *S. cerevisiae* mat formation experiments nor the solution with experimental parameters (figure 3). This supports the hypothesis of low cell–cell adhesion in sliding motility, and justifies setting $\gamma^* = 0$ when comparing the model with experiments.

5. Summary

In this paper, we developed a mathematical model to better understand how mechanics affect yeast biofilm expansion. We were particularly interested in the role of sliding motility and nutrient limitation, features hypothesized to be relevant to mat formation experiments of the budding yeast *S. cerevisiae*. To investigate this, we derived a general multi-phase model for biofilm expansion, treating the biofilm as a mixture of living cells and extracellular fluid. We systematically reduced the model to a one-dimensional axisymmetric form by employing an extensional flow thin-film reduction. By computing numerical solutions, we showed that the thin-film model could reproduce the expansion speed of *S. cerevisiae* mat biofilms. We then confirmed the hypothesis that cell production rate is the strongest determinant of biofilm size in sliding motility. By varying model parameters, we showed that increasing the ability for cells close to the leading edge to consume nutrients and proliferate promotes faster expansion. This can be achieved by decreasing the rates of nutrient diffusion, consumption and depletion, or by increasing the nutrient uptake rate. Finally, we showed that sliding motility is a possible explanation for the ridge formation observed in bacterial or yeast colony biofilms. We found that surface tension slows the movement of cells and nutrients towards the biofilm rim, and thus inhibits ridge formation. Our model confirms that sliding motility is a plausible mechanism for yeast biofilm expansion, and offers a way of quantitatively predicting biofilm growth for other microbial species and environmental conditions.

In addition to these results, our model offers an opportunity to study further biological questions. For example, there are potential links between the characteristic floral morphology of *S. cerevisiae* mats and the stability of solutions to azimuthal perturbations. This provides one avenue for further investigation. Depending on the desired application, the general model also retains the possibility of investigating different mechanisms. For example, the model could be re-scaled to investigate expansion driven by strong adhesion and increased surface tension, rather than sliding motility. A more detailed model could also consider the agar substratum

as viscoelastic, rather than solid. We could then impose continuity of shear stress at biofilm–substratum interface, instead of the zero tangential stress assumed here. The model can also incorporate more complicated cell production mechanisms, for example, ECM production regulated by quorum sensing. It is also possible to include more complicated mechanical behaviour, for example, biofilm viscoelasticity or expansion driven by osmotic swelling. We intend to tackle some of these scenarios in future work, to shed further light on the mechanisms governing biofilm expansion.

Data accessibility. Data and code for this research are available at The University of Adelaide’s Figshare repository, (<https://doi.org/10.25909/5c93294133642>), under the Creative Commons CC BY 4.0 license.

Competing interests. We declare we have no competing interests.

Funding. A.T. received funding from the A. F. Pillow Applied Mathematics Trust, and from the Australian Government under the Research Training Program. J.E.F.G., S.B. and B.J.B. acknowledge funding from the Australian Research Council (ARC), under the grant nos. DE130100031, FT130100484, and DP160102644, respectively. E.L.T. was supported by an Adelaide Graduate Research Scholarship and funding from Wine Australia (GWR Ph1305). J.M.G. and J.F.S. were supported by an ARC grant no. (DP130103547) awarded to V.J.

Acknowledgements. The work used supercomputing resources provided by the Phoenix High Performance Computing service at the University of Adelaide.

References

- Murray JD. 2003 *Mathematical biology II: spatial models and biomedical applications*, 3rd edn. New York, NY: Springer.
- Turing AM. 1952 The chemical basis of morphogenesis. *Phil. Trans. R. Soc. Lond.* **237**, 37–72. (doi:10.1098/rstb.1952.0012)
- Keller EF, Segel LA. 1971 Traveling bands of chemotactic bacteria: a theoretical analysis. *J. Theor. Biol.* **30**, 235–248. (doi:10.1016/0022-5193(71)90051-8)
- Reynolds TB, Fink GR. 2001 Bakers’ yeast, a model for fungal biofilm formation. *Science* **291**, 878–881. (doi:10.1126/science.291.5505.878)
- Tam A, Green JEF, Balasuriya S, Tek EL, Gardner JM, Sundstrom JF, Jiranek V, Binder BJ. 2018 Nutrient-limited growth with non-linear cell diffusion as a mechanism for floral pattern formation in yeast biofilms. *J. Theor. Biol.* **448**, 122–141. (doi:10.1016/j.jtbi.2018.04.004)
- Harshey RM. 2003 Bacterial motility on a surface: many ways to a common goal. *Annu. Rev. Microbiol.* **57**, 249–273. (doi:10.1146/annurev.micro.57.030502.091014)
- Recht J, Martínez A, Torello S, Kolter R. 2000 Genetic analysis of sliding motility in *Mycobacterium smegmatis*. *J. Bacteriol.* **182**, 4348–4351. (doi:10.1128/JB.182.15.4348-4351.2000)
- Martinez LM, Fries BC. 2010 Fungal biofilms: relevance in the setting of human disease. *Curr. Fungal Infect. Rep.* **4**, 266–275. (doi:10.1007/s12281-010-0035-5)
- Flemming H, Wingender J. 2010 The biofilm matrix. *Nat. Rev. Microbiol.* **8**, 623–633. (doi:10.1038/nrmicro2415)
- Ramage G, Rajendran R, Sherry L, Williams C. 2012 Fungal biofilm resistance. *Int. J. Microbiol.* **2012**, 528521. (doi:10.1155/2012/528521)
- Lionakis MS. 2014 New insights into innate immune control of systemic candidiasis. *Med. Mycol.* **52**, 555–564. (doi:10.1093/mmy/myu029)
- Chen L, Noorbakhsh J, Adams RM, Samaniego-Evans J, Agollah G, Nevozhay D, Kuzdzal-Fick J, Mehta P, Balázsi G. 2014 Two-dimensionality of yeast colony expansion accompanied by pattern formation. *PLoS Comput. Biol.* **10**, e1003979. (doi:10.1371/journal.pcbi.1003979)
- Sutherland IW. 2001 The biofilm matrix—an immobilized but dynamic microbial environment. *Trends Microbiol.* **9**, 222–227. (doi:10.1016/S0966-842X(01)02012-1)
- Váchová L, Štovíček V, Hlaváček O, Chernyavskiy O, Štěpánek L, Kubínová L, Palková Z. 2011 Flo11p, drug efflux pumps, and the extracellular matrix cooperate to form biofilm yeast colonies. *J. Cell Biol.* **194**, 679–687. (doi:10.1083/jcb.201103129)
- Beauvais A, Loussert C, Prevost MC, Verstrepen K, Latgé JP. 2009 Characterization of a biofilm-like extracellular matrix in FLO1-expressing *Saccharomyces cerevisiae* cells. *FEMS Yeast Res.* **9**, 411–419. (doi:10.1111/j.1567-1364.2009.00482.x)

16. Shaw T, Winston M, Rupp CJ, Klapper I, Stoodley P. 2004 Commonality of elastic relaxation times in biofilms. *Phys. Rev. Lett.* **93**, 098102. (doi:10.1103/PhysRevLett.93.098102)
17. Cogan NG, Guy RD. 2010 Multiphase flow models of biogels from crawling cells to bacterial biofilms. *Front. Life Sci.* **4**, 11–25. (doi:10.2976/1.3291142)
18. Goffeau A *et al.* 1996 Life with 6000 Genes. *Science* **274**, 546–567. (doi:10.1126/science.274.5287.546)
19. Blankenship JR, Mitchell AP. 2006 How to build a biofilm: a fungal perspective. *Curr. Opin. Microbiol.* **9**, 588–594. (doi:10.1016/j.mib.2006.10.003)
20. Hughes TR. 2002 Yeast and drug discovery. *Funct. Integr. Genomics* **2**, 199–211. (doi:10.1007/s10142-002-0059-1)
21. Tronolone H *et al.* 2018 Diffusion-limited growth of microbial colonies. *Sci. Rep.* **8**, 1–11. (doi:10.1038/s41598-018-23649-z)
22. Nguyen B, Upadhyaya A, van Oudenaarden A, Brenner MP. 2004 Elastic instability in growing yeast colonies. *Biophys. J.* **86**, 2740–2747. (doi:10.1016/S0006-3495(04)74327-1)
23. Seminara A, Angelini TE, Wilking JN, Vlamakis H, Ebrahim S, Kolter R, Weitz DA, Brenner MP. 2012 Osmotic spreading of *Bacillus subtilis* biofilms driven by an extracellular matrix. *Proc. Natl. Acad. Sci. USA* **109**, 1116–1121. (doi:10.1073/pnas.1109261108)
24. Yan J, Nadell CD, Stone HA, Wingreen NS, Bassler BL. 2017 Extracellular-matrix-mediated osmotic pressure drives *Vibrio cholerae* biofilm expansion and cheater exclusion. *Nat. Commun.* **8**, 327. (doi:10.1038/s41467-017-00401-1)
25. Mattei MR, Frunzo L, D'Acunto B, Pechaud Y, Pirozzi F, Esposito G. 2018 Continuum and discrete approach in modeling biofilm development and structure: a review. *J. Math. Biol.* **76**, 945–1003. (doi:10.1007/s00285-017-1165-y)
26. Winstanley HF, Chapwanya M, McGuinness MJ, Fowler AC. 2010 A polymer–solvent model of biofilm growth. *Proc. R. Soc. A* **467**, 1449–1467. (doi:10.1098/rspa.2010.0327)
27. Picioreanu C, van Loosdrecht MCM, Heijnen JJ. 1998 Mathematical modeling of biofilm structure with a hybrid differential-discrete cellular automaton approach. *Biotechnol. Bioeng.* **58**, 101–116. (doi:10.1002/(SICI)1097-0290(19980405)58:1<101::AID-BIT11>3.0.CO;2-M)
28. Matsuura S. 2000 Random growth of fungal colony model on diffusive and non-diffusive media. *Forma* **15**, 309–319.
29. Tronolone H, Gardner JM, Sundstrom JF, Jiranek V, Oliver SG, Binder BJ. 2017 Quantifying the dominant growth mechanisms of dimorphic yeast using a lattice-based model. *J. R. Soc. Interface* **14**, 20170314. (doi:10.1098/rsif.2017.0314)
30. Kawasaki K, Mochizuki A, Matsushita M, Umeda T, Shigesada N. 1997 Modeling spatio-temporal patterns generated by *Bacillus subtilis*. *J. Theor. Biol.* **188**, 177–185. (doi:10.1006/jtbi.1997.0462)
31. Ben-Jacob E, Cohen I, Levine H. 2000 Co-operative self organisation in micro-organisms. *Adv. Phys.* **49**, 395–554. (doi:10.1080/000187300405228)
32. Müller J, van Saarloos W. 2002 Morphological instability and dynamics of fronts in bacterial growth models with nonlinear diffusion. *Phys. Rev. E* **65**, 061111. (doi:10.1103/PhysRevE.65.061111)
33. Wanner O, Gujer W. 1986 A multispecies biofilm model. *Biotechnol. Bioeng.* **28**, 314–328. (doi:10.1002/bit.260280304)
34. Eberl HJ, Parker DF, van Loosdrecht MCM. 2001 A new deterministic spatio-temporal continuum model for biofilm development. *J. Theor. Med.* **3**, 161–175. (doi:10.1080/10273660108833072)
35. Klapper I, Dockery J. 2010 Mathematical description of microbial biofilms. *SIAM Rev.* **52**, 221–265. (doi:10.1137/080739720)
36. Lega J, Passot T. 2003 Hydrodynamics of bacterial colonies: a model. *Phys. Rev. E* **67**, 031906. (doi:10.1103/PhysRevE.67.031906)
37. Giverso C, Verani M, Ciarletta P. 2015 Branching instability in expanding bacterial colonies. *J. R. Soc. Interface* **12**, 20141290. (doi:10.1098/rsif.2014.1290)
38. Cogan NG, Keener JP. 2004 The role of biofilm matrix in structural development. *Math. Med. Biol.* **21**, 147–166. (doi:10.1093/imammb/21.2.147)
39. Anguige K, King JR, Ward JP. 2006 A multi-phase mathematical model of quorum sensing in a maturing *Pseudomonas aeruginosa* biofilm. *Math. Biosci.* **203**, 240–276. (doi:10.1016/j.mbs.2006.05.009)

40. Zhang T, Cogan NG, Wang Q. 2008 Phase-field models for biofilms II: 2-D numerical simulations of biofilm–flow interaction. *Commun. Comput. Phys.* **4**, 72–101.
41. Lindley B, Wang Q, Zhang T. 2012 Multicomponent hydrodynamic model for heterogeneous biofilms: two-dimensional numerical simulations of growth and interaction with flows. *Phys. Rev. E* **85**, 031908. (doi:10.1103/PhysRevE.85.031908)
42. Clarelli F, Di Russo C, Natalini R, Ribot M. 2015 A fluid dynamics multidimensional model of biofilm growth: stability, influence of environment and sensitivity. *Math. Med. Biol.* **33**, 1–25. (doi:10.1093/imammb/dqv024)
43. Fowler AC, Kyrke-Smith TM, Winstanley HF. 2016 The development of biofilm architecture. *Proc. R. Soc. A* **472**, 20150798. (doi:10.1098/rspa.2015.0798)
44. Bees MA, Andresén P, Mosekilde E, Givskov M. 2000 The interaction of thin-film flow, bacterial swarming and cell differentiation in colonies of *Serratia liquefaciens*. *J. Math. Biol.* **40**, 27–63. (doi:10.1007/s002850050004)
45. Angelini TE, Roper M, Kolter R, Weitz DA, Brenner MP. 2009 *Bacillus subtilis* spreads by surfing on waves of surfactant. *Proc. Natl Acad. Sci. USA* **106**, 18109–18113. (doi:10.1073/pnas.0905890106)
46. Ward JP, King JR. 2012 Thin-film modelling of biofilm growth and quorum sensing. *J. Eng. Math.* **73**, 71–92. (doi:10.1007/s10665-011-9490-4)
47. Trinschek S, John K, Thiele U. 2016 From a thin film model for passive suspensions towards the description of osmotic biofilm spreading. *AIMS Mater. Sci.* **3**, 1138–1159. (doi:10.3934/matricsci.2016.3.1138)
48. Trinschek S, John K, Lecuyer S, Thiele U. 2017 Continuous versus arrested spreading of biofilms at solid–gas interfaces: the role of surface forces. *Phys. Rev. Lett.* **119**, 078003. (doi:10.1103/PhysRevLett.119.078003)
49. Trinschek S, John K, Thiele U. 2018 Modelling of surfactant-driven front instabilities in spreading bacterial colonies. *Soft Matter* **14**, 4464–4476. (doi:10.1039/C8SM00422F)
50. Srinivasan S, Kaplan CN, Mahadevan L. 2019 A multiphase theory for spreading microbial swarms and films. *eLife* **8**, e42697. (doi:10.7554/eLife.42697)
51. Eberl HJ, Sudarsan R. 2008 Exposure of biofilms to slow flow fields: the convective contribution to growth and disinfection. *J. Theor. Biol.* **253**, 788–807. (doi:10.1016/j.jtbi.2008.04.013)
52. Palková Z, Váchová L. 2006 Life within a community: benefit to yeast long-term survival. *FEMS Microbiol. Rev.* **30**, 806–824. (doi:10.1111/j.1574-6976.2006.00034.x)
53. Drew DA. 1983 Mathematical modeling of two-phase flow. *Annu. Rev. Fluid Mech.* **15**, 261–291. (doi:10.1146/annurev.fl.15.010183.001401)
54. Maršíková J *et al.* 2017 Metabolic differentiation of surface and invasive cells of yeast colony biofilms revealed by gene expression profiling. *BMC Genom.* **18**, 1–16. (doi:10.1186/s12864-016-3406-7)
55. O’Dea RD, Waters SL, Byrne HM. 2008 A two-fluid model for tissue growth within a dynamic flow environment. *Eur. J. Appl. Math.* **19**, 607–634. (doi:10.1017/S0956792508007687)
56. Batchelor GK. 1967 *An introduction to fluid dynamics*. Cambridge, UK: Cambridge University Press.
57. Franks SJ, Byrne HM, King JR, Underwood JCE, Lewis CE. 2003 Modelling the early growth of ductal carcinoma *in situ* of the breast. *J. Math. Biol.* **47**, 424–452. (doi:10.1007/s00285-003-0214-x)
58. O’Dea RD, Waters SL, Byrne HM. 2010 A multiphase model for tissue construct growth in a perfusion bioreactor. *Math. Med. Biol.* **27**, 95–127. (doi:10.1093/imammb/dqp003)
59. Green JEF, Whiteley JP, Oliver JM, Byrne HM, Waters SL. 2017 Pattern formation in multiphase models of chemotactic cell aggregation. *Math. Med. Biol.* **35**, 319–346. (doi:10.1093/imammb/dqx005)
60. King JR, Oliver JM. 2005 Thin-film modelling of poroviscous free surface flows. *Eur. J. Appl. Math.* **16**, 519–553. (doi:10.1017/S095679250500584X)
61. Chandra J, Kuhn DM, Mukherjee PK, Hoyer LL, McCormick T, Ghannoum MA. 2001 Biofilm formation by the fungal pathogen *Candida albicans*: development, architecture, and drug resistance. *J. Bacteriol.* **183**, 5385–5394. (doi:10.1128/JB.183.18.5385-5394.2001)
62. Howell PD, Scheid B, Stone HA. 2010 Newtonian pizza: spinning a viscous sheet. *J. Fluid Mech.* **659**, 1–23. (doi:10.1017/S0022112010001564)

63. Slade AL, Cremers AE, Thomas HC. 1966 The obstruction effect in the self-diffusion coefficients of sodium and cesium in agar gels. *J. Phys. Chem.* **70**, 2840–2844. (doi:10.1021/j100881a020)
64. Longsworth LG. 1955 12: Diffusion in liquids and the Stokes–Einstein relation. In *Electrochemistry in biology and medicine* (ed. T Shedlovsky), pp. 225–247. New York, NY: John Wiley & Sons, Inc.
65. Stewart PS. 1998 A review of experimental measurements of effective diffusive permeabilities and effective diffusion coefficients in biofilms. *Biotechnol. Bioeng.* **59**, 261–272. (doi:10.1002/(SICI)1097-0290(19980805)59:3<261::AID-BIT1>3.0.CO;2-9)
66. Vicente AA, Dluhý M, Ferreira EC, Mota M, Teixeira JA. 1998 Mass transfer properties of glucose and O₂ in *Saccharomyces cerevisiae* flocs. *Biochem. Eng. J.* **2**, 35–43. (doi:10.1016/S1369-703X(98)00015-1)
67. Crank J. 1984 *Free and moving boundary problems*. Oxford, UK: Science Publications.